Progress In Electromagnetics Research C, Vol. 71, 149–159, 2017

Printed Meander Line MIMO Antenna Integrated with Air Gap, DGS and RIS: A Low Mutual Coupling Design for LTE Applications

Shahanawaz Kamal* **and Anjali Chaudhari**

Abstract—Multiple-input and multiple-output (MIMO) is currently regarded as key technology for long term evolution (LTE) but a critical effect is mutual coupling (S_{21}) due to space constraint in miniaturized design. A compact-size antenna with low mutual coupling would be an ideal choice for better system performance. This paper describes the design of a small-size ($48\times48\,\text{mm}^2$) MIMO antenna system with low mutual coupling for LTE 800 MHz applications. The antenna system comprises of two FR-4 substrate layers; one printed with two meander line antennas (MLAs), the other printed with reactive impedance surface (RIS) and defected ground structure (DGS). The properties of the antenna like S-Parameters, excited surface current distribution, far-field radiation pattern and diversity performance characteristics were studied. The results indicated that MLAs rendered compactness to the system. Introduction of air gap (AG) between the two substrates, DGS and periodic square patches of RIS resulted in 452 MHz bandwidth and mutual coupling of -41.18 dB between antenna elements. The performance of the proposed design compared with other reported geometry has been demonstrated. Parameters including bandwidth, ratio of antenna area/improvement in S_{21}, antenna efficiency and the envelope correlation coefficient were compared. Considering the results, the present system appears to be comparatively more efficient.

1. INTRODUCTION

Long term evolution standard for wireless communication provides high data rates, broader bandwidth and better handoff capabilities [1, 2]. It is an internet protocol (IP) based network offering data rates of 300 Mbps for the downlink channel and 75 Mbps for the uplink channel. MIMO antenna system is employed with multiple antennas at both transmitter and receiver for improving reliability and increasing channel capacity [3, 4]. These have applications in mobile phone, PDA, laptop, etc., where miniaturization is desired. The problem of mutual coupling which arises when multiple antenna elements are placed at close spacing results in mixing of signals emanating from multiple antennas [5, 6]. Reducing mutual coupling between antenna elements is necessary as it results in poor efficiency and affects the channel capacity. A possible solution to overcome this problem is to increase space between antenna elements, but this is impractical in miniature devices as space is a critical limit.

Several techniques have been reported in the literature to reduce mutual coupling in the MIMO antenna system. One approach is to use waveguide metamaterials (WG-MTM). Yang et al. [7] used this technique but found that the reduction was at the cost of increased board area ($76.4 \times 91.0\,\text{mm}^2$) and could achieve bandwidth of only 50 MHz. In another approach by Lee et al. [8] used neutralization line and planar inverted F antenna (PIFA) integrated MIMO system. In this system however with bandwidth of 84 MHz, the resultant radiation pattern did not appear to be optimum. Suwailam et al. [9] could achieve mutual coupling only upto -10.00 dB by using slotted complementary split ring resonators (CSRR). Cheng et al. [10] incorporated electromagnetic bandgap (EBG) in the device design where large

Received 20 November 2016, Accepted 3 February 2017, Scheduled 20 February 2017
* Corresponding author: Shahanawaz Kamal (shahanawazkamal@gmail.com).
The authors are with the Department of Electronics and Telecommunication Engineering, St. Francis Institute of Technology (University of Mumbai), Mumbai 400103, India.

separation between the antenna elements is desired to restrict the surface wave. Hence could not be of use for miniature design. However, Chang et al. [11] and Zhao et al. [12] proved that the addition of decoupling and matching network in a miniature design could reduce mutual coupling between antenna elements. Ghosh et al. [13] introduced meander line resonator to achieve mutual coupling of only upto -10 dB. Ray et al. [14] designed printed antenna consisting of two substrates placed one below the other and separated by air gap in-between. This separation resulted in decreasing the coupling between the two patches. D. Guha and J. Y. Siddiqui [15] obtained attractive tunability characteristics of printed antenna with an air gap in between the substrate and the ground plane. Li et al. [16] designed a defected ground structure (DGS) for reducing mutual coupling but in such a device increment was experienced in back-radiation or decrement in front-to-back ratio. Significant front-to-back radiation ratio was accomplished through the use of metal-backed substrates [17, 18]. Antennas printed on metal-backed substrate have limited efficiency and bandwidth as the radiated field from the image of antenna's electric current cancels out the radiated field from the antenna current itself. In this case, input impedance matching of the antenna becomes difficult as the presence of perfectly electric conductor (PEC) ground plane results in significant increases in the stored electromagnetic energy of the antenna. A possible solution to circumvent this difficulty is to use artificial perfectly magnetic conductor (PMC). Unlike PEC surface, PMC surface allows for the placement of parallel electric currents in their close proximity. The input impedance matching of the antenna becomes easier in case of PMC surface, as the radiated fields add up in-phase. PMC surface however suffers from low overall antenna efficiency as they tend to become lossy and absorb the antenna near-field energy. Mosallaei and Sarabandi [19] utilized the three properties of RIS to minimize mutual coupling effect between the antenna and its image, enhance bandwidth, miniaturize antenna size and improve front-to-back ratio. The three properties of RIS substrate include total power reflection, spatial distributed image representation and ability to store electric or magnetic energy. In MLA, the conductors are folded back and forth to make the overall antenna shorter [20]. Their benefits include, lightweight, small-size, easy to integrate, low fabrication cost and potential for low specific absorption rate (SAR).

The MIMO systems operating in frequency bands higher than 2 GHz are smaller in size than those operating in the low frequency band of 800 MHz. This relaxes the spacing between antenna elements for system operating in high frequency bands. Most of the MIMO systems proposed in literature cover frequency bands that are higher than 2 GHz. In this paper, a compact and economical MIMO antenna system was designed and fabricated considering LTE low frequency bands: 5, 6, 8, 12, 13, 14 and 17 within frequency division duplexing (FDD) mode of operation [21]. Many reported designs have been developed with a focus on a single attribute to reduce the antenna size, enhance bandwidth and improve mutual coupling between antenna elements. In the present work however to design an efficient system multiple attributes notably (a) Air gap (AG) between the two substrates [14, 15], (b) DGS [16], (c) periodic square patches of RIS [19] and (d) MLAs [20] were considered for incorporation into a single geometry. The MIMO antenna system occupying $48 \times 48\,\text{mm}^2$ of board area operates with bandwidth of 44.6% and mutual coupling of -41.18 dB.

2. DESIGN AND CONFIGURATION

The system reported in this paper consists of two independent FR-4 substrate layers placed one below the other and separated by AG of 0.4 mm thickness (Fig. 1). The top and bottom sides of the fabricated antenna design are described in Figs. 2(a) and 2(b). In order to develop a design suitable for miniature devices, it was decided to use a board with area of $48 \times 48\,\text{mm}^2$ and overall height of 2 mm. The antennas were printed on FR-4 substrates of 0.8 mm thickness having a dielectric constant ($\in_r$) of 4.4 and loss tangent ($\tan\delta$) of 0.02. Two MLAs were printed on the top side of the upper substrate (Fig. 3(a)). Periodic square RIS patches of size 4×4 were printed on the top side of the lower substrate (Fig. 3(b)). Ground plane (DGS) was printed on the bottom side of the lower substrate (Fig. 3(c)). The details of the dimension of the system are described in Table 1. The design was fabricated using copper etching technique and fed using SMA connector. The use of FR-4 substrates made the design economical and easy to fabricate.

The two meander line antennas bent opposite to one another was used in the current design to permit cancellation of opposite fields. Li et al. [22] realized DGS by introducing several slits interleaved

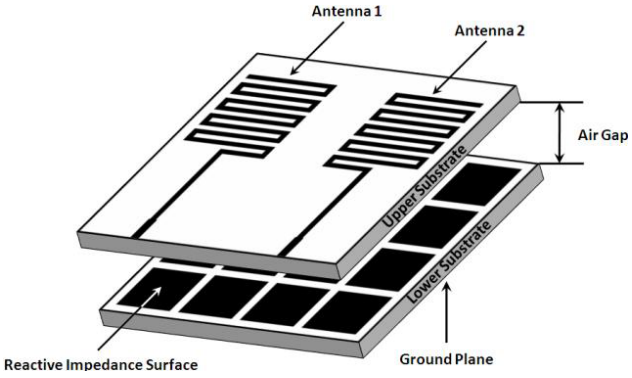

Figure 1. The MIMO antenna system consisting of two independent FR-4 substrates placed one below the other and separated by air gap (AG).

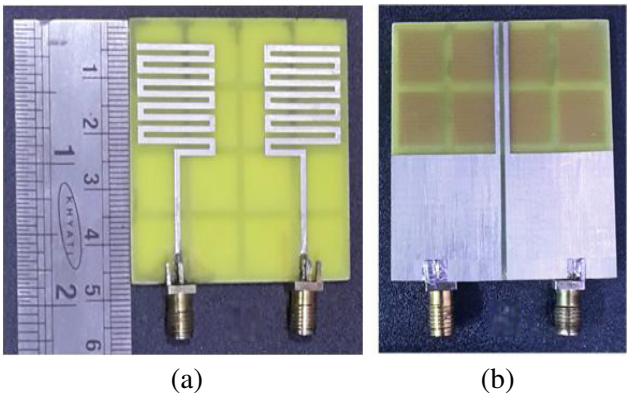

Figure 2. The fabricated MIMO antenna system: (a) Top side and (b) bottom side.

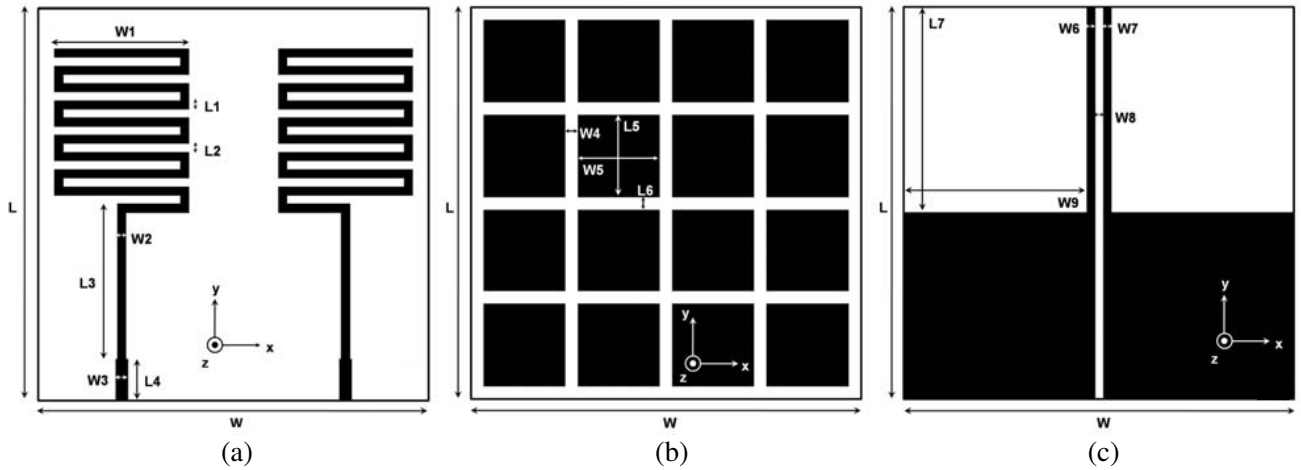

Figure 3. Geometry of the MIMO antenna system: (a) Top side of the upper substrate (MLA), (b) top side of the lower substrate (RIS) and (c) bottom side of the lower substrate (DGS).

Table 1. Parameter values.

Parameter	L	$L1$	$L2$	$L3$	$L4$	$L5$	$L6$	$L7$	W
Value (mm)	48	1.05	1.05	19.05	5	10	1.6	25	48
Parameter	$W1$	$W2$	$W3$	$W4$	$W5$	$W6$	$W7$	$W8$	$W9$
Value (mm)	16.5	1.05	1.5	1.6	10	1	1	1	22.5

with strips which helped in trapping electric current around the series of slits and limiting its flow to other neighboring radiators. Also, the interference currents can be cancelled by the parasitic elements located in the horizontal direction when the two elements are fed simultaneously [23]. By following this, DGS was realized in the current design by introducing ground plane cuts and split with the length of the arm. Parametric simulation studies were performed for designing DGS, AG and RIS patches and discussed in the next section.

3. RESULTS AND DISCUSSION

3.1. *S*-Parameters

The performance of MIMO antenna system was optimized and analyzed using Ansoft HFSS [24]. The DGS was designed by investigating four cases notably (a) without: ground plane cuts and split with the length of the arm, (b) with: ground plane cuts; without: split with the length of the arm, (c) without: ground plane cuts; with: split with the length of the arm, (d) with: ground plane cuts and split with the length of the arm (Fig. 4). It is evident from the results shown in Fig. 4 that case (d) satisfies the requirement of antenna resonant frequency at 800 MHz with a better reduction in mutual coupling. Hence DGS realized by introducing ground plane cuts and split with the length of the arm was selected for further analysis. Fig. 5 describes the simulation results for *S*-Parameters of MIMO integrated with AG, DGS and RIS. Parametric simulation studies were performed with different AG thicknesses (1 mm, 0.8 mm, 0.2 mm and 0.4 mm). It is evident from the curves that AG of size 0.4 mm gave optimum mutual coupling. Hence, AG = 0.4 mm was selected for further analysis. Parametric simulation studies were also carried out for deciding the design of RIS patches (Table 2).

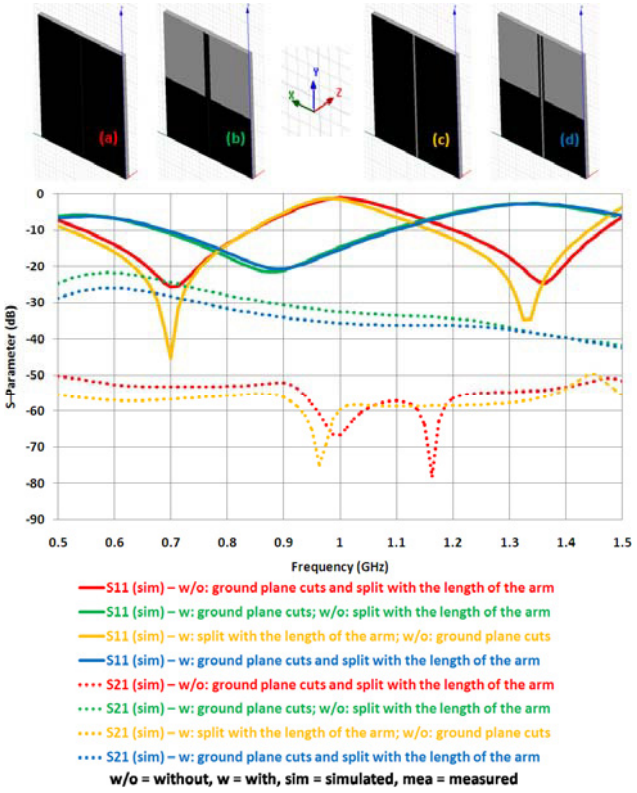

Figure 4. Parametric simulation studies for the design of DGS.

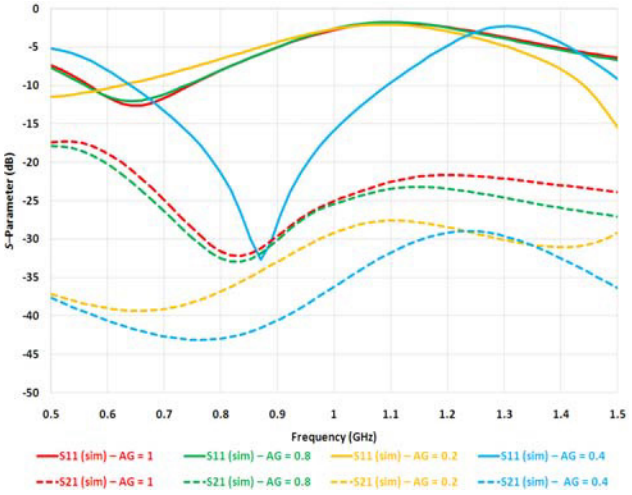

Figure 5. Simulated *S*-Parameters with variation in thickness of AG (mm) for the MIMO (w: AG, DGS and RIS).

In order to check effects of AG, DGS and RIS on *S*-parameters, four distinct cases of the MIMO antenna system were investigated notably (a) without: AG, DGS and RIS, (b) with: DGS; without: AG and RIS, (c) with: DGS and RIS; without: AG and (d) with: AG, DGS and RIS (Fig. 6). The MIMO (with: AG, DGS and RIS) showed S_{11} value of -33.94 dB at 0.874 GHz and covered the frequencies of 0.641 GHz to 1.093 GHz. The results also yielded S_{21} value of -41.18 dB at 0.874 GHz.

Similar measurement studies were carried out on the physical MIMO (with: AG, DGS and RIS). Measurement of the fabricated system was conducted using Rohde & Schwarz's VNA. Mutual coupling between the two antenna elements was determined through the computation of S_{21}. A 50 Ω termination

Table 2. Parametric simulation studies for the design of RIS.

$L \times W$ (mm)	No. of RIS patches	No. of meander line turns	Freq (GHz)	$\lvert S_{11}\rvert$ (dB)	$\lvert S_{21}\rvert$ (dB)
48×48	16	10	0.874	33.94	41.18
48×48	64	10	0.820	11.40	32.85
50×50	16	12	0.614	22.08	15.07
50×50	64	12	0.505	12.35	25.05
43.89×50	56	10	0.620	13.87	27.41

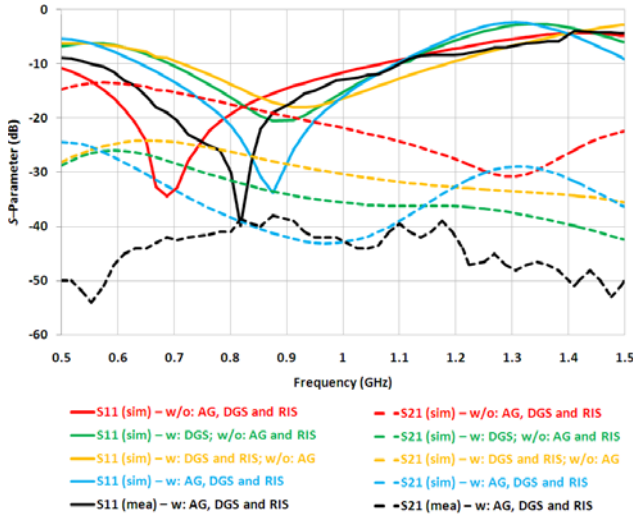

Figure 6. Simulated and measured S-Parameters of the MIMO.

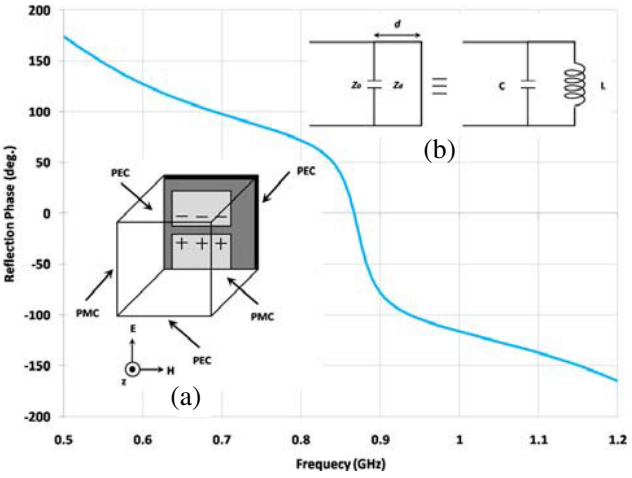

Figure 7. Simulated reflection phase of RIS substrate for the MIMO (w: AG, DGS and RIS): (a) Unit cell of RIS enclosed by PEC and PMC walls and illuminated by a normal incident plane wave and (b) parallel LC equivalent model.

was used on port 2 during the S_{21} measurement of the fabricated system. The results showed S_{11} value of -39.87 dB at 0.810 GHz with approximately 50% operational bandwidth and mutual coupling of -40.00 dB (Fig. 6). The shift in the resonant frequency was due to the hand soldering, the tolerances of the SMA connector and the termination resistance.

DGS realized by introducing ground plane cuts and split with the length of the arm disturbed the shield current distribution leading to a controlled propagation of electromagnetic (EM) waves thereby reducing mutual coupling. In order to overcome the drawback of DGS, i.e., decrement in front-to-back radiation ratio, RIS was introduced in the design.

The periodicity of RIS square patches on a PEC-backed dielectric substrate was selected to be smaller than the wavelength. This enabled differentiation between RIS structures from frequency selective surfaces (FSS). It was reported that RIS with moderate value of impedance ($\eta = jv$) reduces the mutual coupling between the patch radiator and the ground plane [19]. Also, placing antennas over RIS provides wider bandwidth. Considering a unit cell of RIS, the square patch acts as a shunt capacitor placed at a distance (d) from a short circuited dielectric load transmission line, which can be modeled by a lumped shunt inductor parallel to the capacitor (Figs. 7(a) and 7(b)). The curve described in Fig. 7 shows that the parallel LC circuit behaves as an open circuit or PMC at resonance whereas below resonance the curve appears to be inductive and above resonance capacitive. An inductive RIS is capable of storing magnetic energy thereby increasing the total inductance of the patch and providing compensation for electric energy stored in near-field of antennas. Thus antenna miniaturization is achieved.

3.2. Surface Current Distribution

The excited surface current distributions of four distinct cases of the MIMO antenna system are depicted in Figs. 8(a)–8(d). The results were depicted with antenna 1 as the excited and antenna 2 as the 50 Ω matched terminated. On the MIMO (w/o: AG, DGS and RIS), surface current was coupled from antenna 1 to antenna 2 through the ground plane. However, the MIMO (w: AG, DGS and RIS) showed significant suppression of current. A similar effect was observed with antenna 2 as the excited and antenna 1 as the 50 Ω matched terminated. Hence it was concluded that AG, DGS and RIS can significantly reduce mutual coupling between antenna elements of the MIMO antenna system.

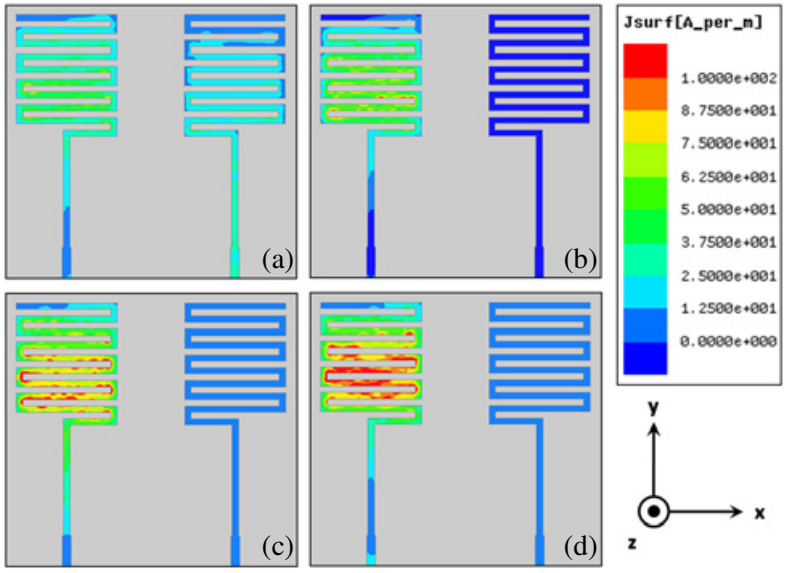

Figure 8. Excited surface current distribution of the MIMO: (a) w/o: AG, DGS and RIS, (b) w: DGS; w/o: AG and RIS, (c) w: DGS and RIS; w/o: AG and (d) w: AG, DGS and RIS.

3.3. Far-Field Radiation Pattern

Figure 9 shows measured radiation pattern of the MIMO (w: AG, DGS and RIS) at 0.810 GHz, which represents the total field amplitude combining E_θ and E_φ components ($E_{\text{total}} = \sqrt{(E_\theta^2 + E_\varphi^2)}$). A 50 Ω termination was used on port 2 during the radiation pattern measurement of antenna 1 and vice versa. The radiation patterns in the E-plane and H-plane of antenna 1 and antenna 2 are the mirror images of each other which indicate that the proposed MIMO has good pattern diversity characteristics. In E-plane and H-plane, the radiation patterns are nearly omnidirectional. At resonant frequency, the MIMO (with: AG, DGS and RIS) showed peak gain value of 6.23 dBi (simulated) and 5.81 dBi (measured),

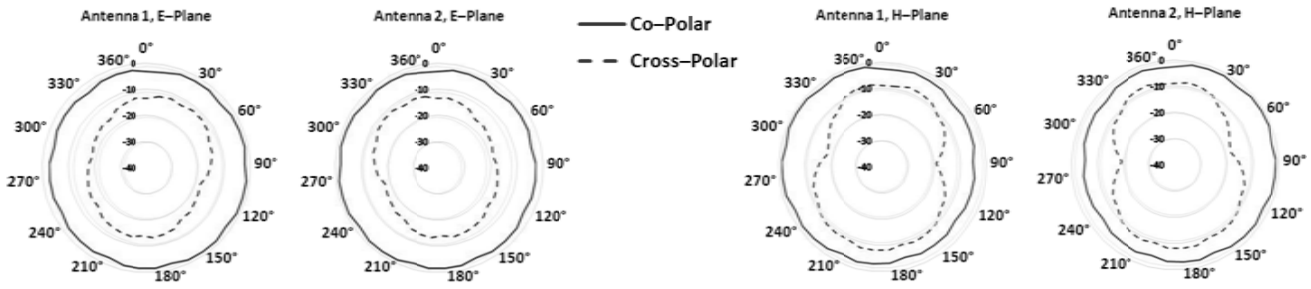

Figure 9. Measured radiation pattern of the MIMO (w: AG, DGS and RIS) at 0.810 GHz.

which is little higher than a regular antenna (Fig. 10). Hence, the MIMO is capable of providing high channel capacity.

3.4. Diversity Performance

The diversity performance of MIMO antenna system is usually evaluated by envelope correlation coefficient between the ith and jth antenna elements (ρ_{eij}) and mean effective gain (MEG) [25]. The diversity parameters were evaluated using CST MWS simulation software [26] and were also measured. In order to calculate ρ_{eij} and MEG of a particular antenna element, the following criteria are widely used [27],

$$\rho_{eij} < 0.5 \quad \text{and} \quad \frac{\text{MEG}_i}{\text{MEG}_j} \cong 1 \tag{1}$$

where, MEG_i and MEG_j denote the ratios of the average receiving power to the total average incident power of the ith and jth antenna elements, respectively. MEG can be expressed as [28],

$$\text{MEG} = \int_0^{2\pi} \int_0^{\pi} \left[\frac{\text{XPR}}{1+\text{XPR}} \cdot G_\theta(\theta,\varphi) P_\theta(\theta,\varphi) + \frac{1}{1+\text{XPR}} \cdot G_\varphi(\theta,\varphi) P_\varphi(\theta,\varphi) \right] \sin(\theta) d\theta d\varphi \tag{2}$$

where, XPR denotes cross-polarization power ratio of the propagation environment. $G_\theta(\theta,\varphi)$ and $G_\varphi(\theta,\varphi)$ are the power patterns of θ and φ polarizations, respectively. $P_\theta(\theta,\varphi)$ and $P_\varphi(\theta,\varphi)$ denote the angular density functions of the θ and φ polarizations, respectively. $P_\theta(\theta,\varphi)$ and $P_\varphi(\theta,\varphi)$ are subjected to the following equations [29],

$$\int_0^{2\pi} \int_0^{\pi} P_\theta(\theta,\varphi) \sin(\theta) d\theta d\varphi = 1 \tag{3}$$

$$\int_0^{2\pi} \int_0^{\pi} P_\varphi(\theta,\varphi) \sin(\theta) d\theta d\varphi = 1 \tag{4}$$

By using far-field patterns, ρ_{eij} can be expressed as [29],

$$\rho_{eij} \approx \frac{\left[\int_0^{2\pi} \int_0^{\pi} \left\{ \text{XPR} \cdot E_{\theta i}(\theta,\varphi) E_{\theta j}^*(\theta,\varphi) P_\theta(\theta,\varphi) + E_{\varphi i}(\theta,\varphi) E_{\varphi j}^*(\theta,\varphi) P_\varphi(\theta,\varphi) \right\} \sin(\theta) d\theta d\varphi \right]^2}{\begin{array}{l} \left[\int_0^{2\pi} \int_0^{\pi} \left\{ \text{XPR} \cdot E_{\theta i}(\theta,\varphi) E_{\theta i}^*(\theta,\varphi) P_\theta(\theta,\varphi) + E_{\varphi i}(\theta,\varphi) E_{\varphi i}^*(\theta,\varphi) P_\varphi(\theta,\varphi) \right\} \sin(\theta) d\theta d\varphi \right] \\ \cdot \left[\int_0^{2\pi} \int_0^{\pi} \left\{ \text{XPR} \cdot E_{\theta j}(\theta,\varphi) E_{\theta j}^*(\theta,\varphi) P_\theta(\theta,\varphi) + E_{\varphi j}(\theta,\varphi) E_{\varphi j}^*(\theta,\varphi) P_\varphi(\theta,\varphi) \right\} \sin(\theta) d\theta d\varphi \right] \end{array} \tag{5}$$

where, $E_{\theta i}(\theta,\varphi)$ and $E_{\theta j}(\theta,\varphi)$ are the electric field patterns of the ith and jth antenna elements in the θ polarization, respectively. $E_{\varphi i}(\theta,\varphi)$ and $E_{\varphi j}(\theta,\varphi)$ are the electric field patterns of the ith and jth antenna elements in the φ polarization, respectively.

For a mobile terminal moving in the horizontal plane, the azimuth angle of the incident wave is assumed as uniform distribution while the elevation angle of the incident wave is assumed as Gaussian distribution. Also, the distribution of azimuth and elevation angle with the same polarization is assumed to be independent. Hence $P_\theta(\theta,\varphi)$ and $P_\varphi(\theta,\varphi)$ can be expressed as,

$$P_\theta(\theta,\varphi) = \lambda_\theta \exp\left\{ \frac{\left[\theta - \left(\frac{\pi}{2} - \mu_v\right)\right]^2}{2\sigma_v^2} \right\}, \quad 0 \le \theta \le \pi \tag{6}$$

$$P_\varphi(\theta,\varphi) = \lambda_\varphi \exp\left\{ \frac{\left[\theta - \left(\frac{\pi}{2} - \mu_h\right)\right]^2}{2\sigma_h^2} \right\}, \quad 0 \le \theta \le \pi \tag{7}$$

where, λ_θ and λ_φ are the proportional constants that can be obtained according to Eqs. (3) and (4), respectively. μ_v and μ_h are the mean elevation angles of the θ and φ polarizations, and σ_v^2 and σ_h^2 are the standard deviations of the θ and φ polarizations. The values of these scenario parameters are presented in [27].

Envelope correlation coefficient has been evaluated by using the far-field patterns of the MIMO (Fig. 11). At resonant frequency, simulated and measured results showed $\rho_{eij} < 0.5$. MEGs for different

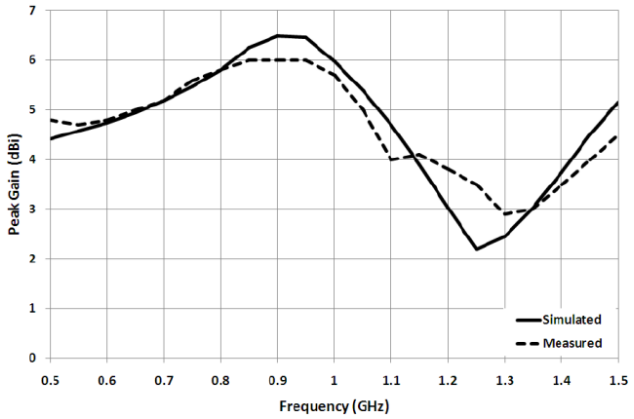

Figure 10. Simulated and measured peak gain of the MIMO (w: AG, DGS and RIS).

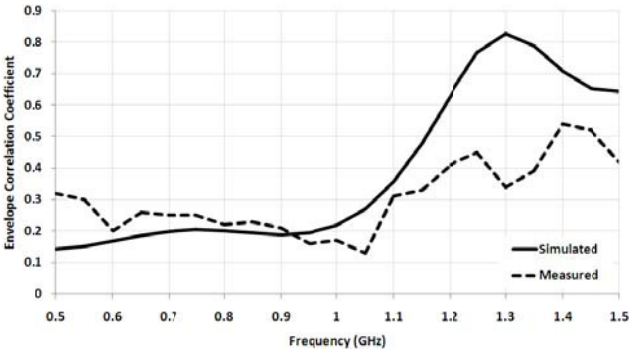

Figure 11. Simulated and measured envelope correlation coefficient of the MIMO (w: AG, DGS and RIS).

Table 3. Computed MEGs at 0.874 GHz for different XPRs.

Indoor (XPR = 5 dB)		**Outdoor (XPR = 1 dB)**		**Isotropic (XPR = 0 dB)**	
MEG1	**MEG2**	**MEG1**	**MEG2**	**MEG1**	**MEG2**
−4.883762	−4.8833958	−3.3539145	−3.3538745	−3.0103	−3.0103

XPRs at 0.874 GHz was calculated (Table 3). These results satisfy the criteria expressed in Eq. (1). Hence, the MIMO system is capable of providing good diversity performance.

Apparent diversity gain (G_{app}) is also an important diversity parameter which can be evaluated using the following equation [30, 31],

$$G_{app} = 10e_\rho \quad \text{with} \quad e_\rho = \sqrt{1 - |\rho_{ij}|} \tag{8}$$

where, e_ρ is an expression for the correlation efficiency, and ρ_{ij} is the correlation coefficient. At resonant frequency, diversity gains of 9.53 dB (simulated) and 9.31 dB (measured) were obtained (Fig. 12).

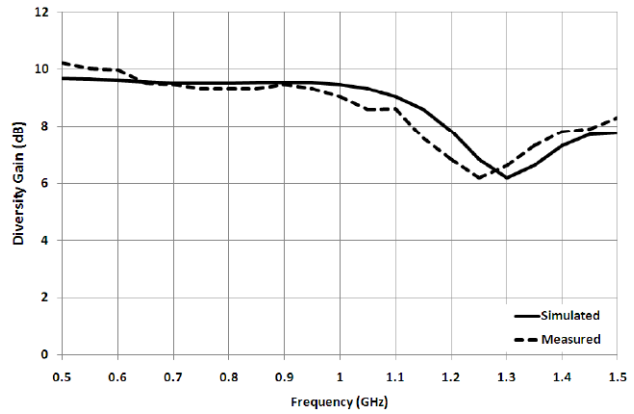

Figure 12. Simulated and measured diversity gain of the MIMO (w: AG, DGS and RIS).

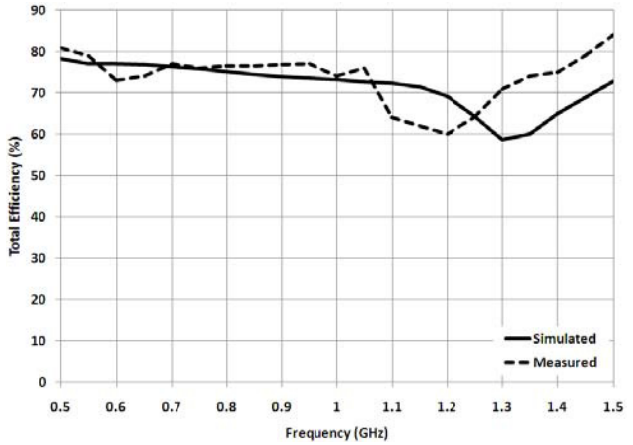

Figure 13. Simulated and measured total efficiency of the MIMO (w: AG, DGS and RIS).

The total efficiency (η_{total}) of MIMO antenna system is given by [32],

$$\eta_{\text{total}} = \eta\left(1 - |S_{11}|^2 - |S_{21}|^2\right) \tag{9}$$

where, η is the radiation efficiency of the antenna. The simulated and measured results depicted as curves in Fig. 13 show that the MIMO (w: AG, DGS and RIS) had an efficiency of approximately 75%. The effective diversity gain (EDG) of the antenna system was determined by multiplying the diversity gain with total antenna efficiency. At resonant frequency, EDG of 7.05 dB was obtained for the MIMO (w: AG, DGS and RIS).

3.5. Performance of the Proposed Configuration and Other Reported Configurations

Table 4 shows the results of various approaches adopted for reducing mutual coupling between antenna elements in a printed antenna. Parameters including bandwidth, ratio of antenna area/improvement in S_{21}, antenna efficiency and envelope correlation coefficient were compared. The proposed MIMO antenna system with miniaturized design offers a wide bandwidth and reduced mutual coupling.

Table 4. Performance of the proposed configuration and other reported configurations.

Ref. No.	Approach	F (GHz)	BW (MHz)	Antenna Area (mm^2)	Improvement in S_{21} (dB)	Antenna Area (mm^2) / Improvement in S_{21} (dB)	Antenna Efficiency	ρ_{eij}
[7]	WG-MTM	3.5	50	6952.4	20.00	347.62	NR	NR
[8]	Neutralization Line + PIFA	2.4	84	3750	40.00	93.75	80%	NR
[9]	Slotted CSRR	5.0	500	4680	10.00	468	NR	NR
[10]	EBG	2.1	45	10000	48.00	208.34	NR	NR
		2.5	71					
[11]	Decoupling Technique	2.45	200	990	35	28.29	> 75%	NR
[12]		2.6	300	9180	20.00	459	83%	0.27
[13]	Meander Line Resonator	2.8	200	610.08	10.00	61.01	NR	NR
[16]	DGS	2.1	800	3000	10.00	300	NR	NR
		5.4	400		20.00	150		
[33]	PIFA	0.74	124	7200	6.00	1200	> 50%	0.925
[34]	T-shaped common radiator	0.765	41	900	17.5	51.43	70%	< 0.05
[35]	Additional resistive sheets	0.9	2000	4600	40.00	115	> 80%	NR
		2.4						
Proposed	AG + DGS + RIS	0.8	452	2304	41.18	55.94	75%	0.19

F = Frequency, BW = Bandwidth, ρ_{eij} = Envelope correlation coefficient, NR = Not Reported

4. CONCLUSION

In this paper, a meander line based MIMO antenna system with low mutual coupling between antenna elements was fabricated to be used in the 800 MHz frequency band of LTE standard. The system occupied $48 \times 48\,mm^2$ of board area and overall height of 2 mm. Mutual coupling between antenna elements was reduced by introducing AG, DGS and RIS. The simulation results showed operational bandwidth of 44.6% and mutual coupling of -41.18 dB. The diversity performance with respect to envelope correlation coefficient, mean effective gain, apparent diversity gain, total efficiency and effective diversity gain was verified. In order to compare with the other reported system, parameters including bandwidth, ratio of antenna area/improvement in S_{21}, antenna efficiency and envelope correlation coefficient were considered. The geometry reported in the paper appears to be comparatively more efficient.

ACKNOWLEDGMENT

The authors would like to thank Dr. Girish Kumar, Department of Electrical Engineering, Indian Institute of Technology Bombay, Mumbai 400076, India, for the antenna measurement.

REFERENCES

1. Garg, V. K., *Wireless Communications and Networks*, Morgan Kaufmann Publishers, Elsevier, 2007.
2. Larmo, A., M. Lindstrom, M. Meyer, G. Pelletier, J. Torsner, and H. Wiemann, "The LTE link-layer design," *IEEE Communications Magazine*, Vol. 47, No. 4, 52–59, Apr. 2009.
3. Foschini, G. J. and M. J. Gans, "On limits of wireless communications in a fading environment when using multiple antennas," *Wireless Personal Communications*, Vol. 6, 311–335, Mar. 1998.
4. Telatar, E., "Capacity of multi-antenna Gaussian channels," *European Transactions on Telecommunications*, Vol. 10, No. 6, 585–595, Nov. 1999.
5. Ludwig, A., "Mutual coupling, gain and directivity of an array of two identical antennas," *IEEE Transactions on Antennas and Propagation*, Vol. 24, No. 6, 837–841, Nov. 1976.
6. Lau, B. K. and Z. Ying, "Antenna design challenges and solutions for compact MIMO terminals," *IEEE International Workshop on Antenna Technology (iWAT)*, 70–73, Apr. 2011.
7. Yang, X. M., X. G. Liu, X. Y. Zhou, and T. J. Cui, "Reduction of mutual coupling between closely packed patch antennas using waveguided metamaterials," *IEEE Antennas and Wireless Propagation Letters*, Vol. 11, 389–391, Apr. 2012.
8. Lee, C. H., S. Y. Chen, and P. Hsu, "Integrated dual planar inverted-F antenna with enhanced isolation," *IEEE Antennas and Wireless Propagation Letters*, Vol. 8, 963–965, Aug. 2009.
9. Bait-Suwailam, M. M., O. F. Siddiqui, and O. M. Ramahi, "Mutual coupling reduction between microstrip patch antennas using slotted-complementary split-ring resonators," *IEEE Antennas and Wireless Propagation Letters*, Vol. 9, 876–878, Sep. 2010.
10. Cheng, C., F. Zhang, Y. Wan, and F. Zhang, "Miniaturized high-isolation dual-frequency orthogonally polarized patch antenna using compact electromagnetic bandgap filters," *International Journal of Antennas and Propagation*, Apr. 2014.
11. Chen, S. C., Y. S. Wang, and S. J. Chung, "A decoupling technique for increasing the port isolation between two strongly coupled antennas," *IEEE Transactions on Antennas and Propagation*, Vol. 56, No. 12, 3650–3658, Dec. 2008.
12. Zhao, L., L. K. Yeung, and K. L. Wu, "A coupled resonator decoupling network for two-element compact antenna arrays in mobile terminals," *IEEE Transactions on Antennas and Propagation*, Vol. 62, No. 5, 2767–2778, May 2014.
13. Ghosh, J., S. Ghosal, D. Mitra, and S. R. Bhadra Chaudhuri, "Mutual coupling reduction between closely placed microstrip patch antenna using meander line resonator," *Progress In Electromagnetics Research Letters*, Vol. 59, 115–122, 2016.
14. Ray, K. P., S. Ghosh, and K. Nirmala, "Multilayer multiresonator circular microstrip antennas for broadband and dual-band operations," *Microwave and Optical Technology Letters*, Vol. 47, 489–494, Dec. 2005.
15. Guha, D. and J. Y. Siddiqui, "Resonant frequency of equilateral triangular microstrip antenna with and without air gap," *IEEE Transactions on Antennas and Propagation*, Vol. 52, No. 8, 2174–2178, Aug. 2004.
16. Li, L., Y. Yu, and L. Yi, "Mutual coupling reduction between printed dual-frequency antenna arrays," *Progress In Electromagnetics Research Letters*, Vol. 59, 63–69, 2016.
17. Sievenpiper, D., L. Zhang, R. F. J. Broas, N. G. Alexópoulos, and E. Yablonovitch, "High-impedance electromagnetic surfaces with a forbidden frequency band," *IEEE Transactions on Microwave Theory Techniques*, Vol. 47, 2059–2074, Nov. 1999.

18. Yeo, J. and R. Mittra, "Bandwidth enhancement of multiband antennas using frequency selective surfaces for ground planes," *IEEE International Symposium on Antennas and Propagation Society*, Vol. 4, 366–369, Jul. 2001.
19. Mosallaei, H. and K. Sarabandi, "Antenna miniaturization and bandwidth enhancement using a reactive impedance substrate," *IEEE Communications Magazine*, Vol. 52, No. 9, 2403–2414, Sep. 2004.
20. Marrocco, G., "Gain-optimized self-resonant meander line antennas for RFID applications," *IEEE Antennas and Wireless Propagation Letters*, Vol. 2, 302–305, Jan. 2003.
21. 3GPP TS 36.101, V8.3.0, EUTRA User Equipment Radio Transmission and Reception, 2008.
22. Li, H., J. Xiong, and S. He, "A compact planar MIMO antenna system of four elements with similar radiation characteristics and isolation structure," *IEEE Antennas and Wireless Propagation Letters*, Vol. 8, 1107–1110, Oct. 2009.
23. Min, K. S., D. J. Kim, and Y. M. Moon, "Improved MIMO antenna by mutual coupling suppression between elements," *The European Conference on Wireless Technology*, 125–128, Paris, France, Oct. 2005.
24. ANSYS HFSS ver. 13.0.0, ANSYS, Canonsburg, PA, USA, 2011, [online], available: http://www.ansys.com.
25. Ghosh, S., T. N. Tran, and T. Le-Ngoc, "Miniaturized four-element diversity PIFA," *IEEE Antennas Wireless Propagation Letters*, Vol. 12, 396–400, Mar. 2013.
26. CST Microwave Studio, [online], available: http://www.cst.com.
27. Karaboikis, M. P., V. C. Papamichael, G. F. Tsachtsiris, C. F. Soras, and V. T. Makios, "Integrating compact printed antennas onto small diversity/MIMO terminals," *IEEE Transactions on Antennas and Propagation*, Vol. 56, No. 7, 2067–2078, Jul. 2008.
28. Taga, T., "Analysis for mean effective gain of mobile antennas in land mobile radio environments," *IEEE Transactions on Vehicular Technology*, Vol. 39, 117–131, May 1990.
29. Taga, T., "Analysis of correlation characteristics of antenna diversity in land mobile radio environments," *Electronics and Communications in Japan, Part I*, Vol. 74, No. 8, 101–116, 1991.
30. Schwartz, M., W. R. Bennett, and S. Stein, *Communication System and Techniques*, 470–474, McGraw-Hill, New York, 1965.
31. Pierce, J. N. and S. Stein, "Multiple diversity with non independent fading," *Proceedings of the IRE*, Vol. 48, 89–104, Jan. 1960.
32. Rao, Q. and K. Wilson, "Design, modeling and evaluation of a multiband MIMO/diversity antenna system for small wireless mobile terminals," *IEEE Transactions on Components, Packaging and Manufacturing Technology*, Vol. 1, 410–419, Mar. 2011.
33. Zhang, S., A. A. Glazunov, Z. Ying, and S. He, "Reduction of the envelope correlation coefficient with improved total efficiency for mobile LTE MIMO antenna arrays: Mutual scattering mode," *IEEE Transactions on Antennas and Propagation*, Vol. 61, No. 6, 3280–3291, Jun. 2013.
34. Lee, B., F. J. Harackiewicz, and H. Wi, "Closely mounted mobile handset MIMO antenna for LTE13 band application," *IEEE Antennas and Wireless Propagation Letters*, Vol. 13, 411–414, Feb. 2014.
35. Yetisir, E., C. C. Chen, and J. L. Volakis, "Low profile UWB 2-port antenna with high isolation," *IEEE Antennas and Wireless Propagation Letters*, Vol. 13, 55–58, 2014.